Exploring oxygen diffusion and respiration in pome fruits using non-destructive gas in scattering media absorption spectroscopy

Manju Joseph[1], Robbe Van Beers[1], Annelies Postelmans, Bart Nicolai[1,2] and Wouter Saeys[1]

[1]KU Leuven, Department of Biosystems, MeBioS, Kasteelpark Arenberg 30, 3001, Leuven, Belgium

[2]VCBT - Flanders Centre of Postharvest Technology, Willem de Croylaan 42, 3001 Leuven, Belgium

ABSTRACT

Pome fruit stored under controlled atmosphere (CA) often suffer from hypoxia due to a mismatch between the O_2 level in the storage rooms and the fruit's O_2 consumption. Fruit response based O_2 sensing and control could be an efficient approach to reduce the hypoxia-related physiological disorders and therefore increase the shelf life of the stored fruits. The aim of this research was to validate and evaluate the application of nondestructive gas in scattering media absorption spectroscopy (GASMAS) O_2 sensing in fruit post-harvest. In a first stage, the system involving a tunable diode laser was validated on a fruit mimicking multilayer model system where high correlations were observed between the measured and reference O_2 partial pressure (r^2 ≥0.9). Next, the GASMAS sensor was evaluated on two apple cultivars (*Malus x domestica* 'Golden Delicious', *Malus x domestica* 'Nicoter') and one pear cultivar (*Pyrus x communis* 'Conference'). The observed GASMAS signal from the 'Golden delicious' apples was nearly 2 times higher than the signal from the 'Nicoter' apples and nearly 5 times higher than from the 'Conference' pears. Next, GASMAS measurements were performed on water submerged 'Golden Delicious' apple and 'Conference' pear samples to investigate the difference in O_2 consumption in these fruits. It was found that the calculated relative O_2 changes during respiration and the evolution of the O_2 partial pressure after nitrogen treatment for both of these fruit were different. It was hypothesized that these findings may be attributed to differences in fruit porosity. Finally, the influence of skin and additional surface coating on gas exchange was studied by immersing unpeeled, peeled and

coated samples in gaseous nitrogen for 2 h prior to the measurement. The coating was found to reduce the gas exchange compared to unpeeled samples which already exhibited a lower exchange rate than the peeled samples. Based on these findings it was concluded that introduction of non-destructive GASMAS O_2 sensors in CA storage of pome fruits could help in reducing hypoxia related disorders, thereby improving the quality and shelf-life of stored fruit.

Keywords: hypoxia, O_2 diffusion, GASMAS, liquid phantom model, Monte Carlo simulations, CA.

1. INTRODUCTION

Oxygen is a key element in many metabolic pathways in plants, including respiration. Respiration results in physiological as well as biochemical changes in living tissues. In climacteric fruit like pome fruit the respiration rate surges in concert with the ethylene production rate at the onset of ripening (Busatto et al., 2017). To prevent fast ripening and senescence of pome fruit, controlled atmosphere (CA) storage is commonly used to reduce ethylene biosynthesis and respiration. This is achieved by reducing the O_2 level of the cool store while increasing the CO_2 level (Thompson and Bishop, 2016). Because of the resistance of the skin and cortex tissue with respect to diffusion, O_2 and CO_2 gradients develop and the local O_2 partial pressure may decrease to levels beyond which the respiration metabolism stalls and fermentation takes over. The ATP yield of the latter pathway is much lower and at some point, the fruit can no longer sustain essential maintenance processes such as membrane repair. This may lead to loss of cell integrity, browning reactions may occur due to oxidation of phenolic substrates (Ho et al., 2013) and internal browning symptoms. Novel storage methodologies such as dynamic controlled atmosphere (DCA) storage (Bessemans et al., 2016) impose even much lower O_2 levels compared to conventional CA storage. Knowledge of local O_2 and CO_2 partial pressure inside the fruit during hypoxic storage is, therefore, essential to understand the changes in the fruit physiology during controlled atmosphere storage and further develop novel dynamic controlled atmosphere methodologies.

Several sensor principles to measure the local O_2 partial pressure in a variety of plant organs have been evaluated in the literature (van Dongen and Licausi, 2014). Traditional polarographic sensor based O_2 sensing and profiling was common in earlier days. Macro or micro electrodes are inserted into the plant organ and the resulting electric current which is proportional to the amount of oxygen in the tissue is measured (Armstrong,1993). Gas sampling from an interior surface of the plant tissue and then analyzing it using gas chromatography is an another method of internal oxygen sensing (Lammertyn et al., 2001; Cindy et al., 2012; van Dongen and Licausi, 2014). More recently, an optical O_2 sensing technique was developed based on an oxygen-sensitive fluorophore in a foil or fiber tip. By placing the sensor foil on a biological sample or inserting fluorescent optical needle into the tissue intracellular oxygen concentration can be obtained (Ho et al., 2010; Rolletschek and Liebsch, 2017). However, all these methods are destructive and less applicable for internal oxygen measurements of fruit. A noninvasive measurement of internal gas concentrations in pome fruit tissue is very difficult, though, as inserting, for example, a needle oxygen probe may cause leakage of oxygen along the shaft of the needle and invalidate the measurements. Alternatively, the focus has been on gas transport models at multiple scales (Ho et al., 2008) that have been validated to some extent. However, there is a need for noninvasive methods to measure the local O_2 partial pressure in pome fruit in response to different storage atmospheres to further validate these models.

Gas in scattering media absorption spectroscopy (GASMAS), a technique based on tunable diode laser absorption spectroscopy (TDLAS), has been proposed as an alternative for non-destructive detection of oxygen in highly scattering media (Sjöholm et al., 2001).The gas absorption features are 10,000 times sharper than those of the surrounding bulk media and each gas has its own wavelength-dependent absorption imprint. This promotes selective detection of a gas of interest in a turbid medium. A wavelength tuned and frequency modulated diode laser paired with a highly sensitive detector helps to perform selective and sensitive detection of gases from the noisy

scattering media in GASMAS. Although the technique is predominantly used to measure oxygen and water vapor (Svanberg, 2013), it has also been validated for carbon dioxide (Svensson and Shen, 2010) and methane (Ding et al., 2014). GASMAS has already been applied in various areas as diverse as food packaging (Boonruang et al., 2012; Lewander et al., 2008), pharmaceutical preparations (Svensson et al., 2008), diagnostics of lungs and body cavities (Persson et al., 2007; Lewander et al., 2011) and in the construction of materials (Zhang and Svanberg, 2016). In the postharvest domain, it has been applied to study the role of fruit skin on the exchange of oxygen (Persson et al., 2006), oxygen signal intensity variation during tropical fruit ripening (Zhang et al., 2014) and to investigate the pressure changes after vacuum impregnation of apple (Tylewicz et al., 2012). However, most of these experiments were performed on high porosity fruit like apple where the signal to noise ratio is comparatively high, while lower porosity fruit are more susceptible to hypoxia. Therefore, it would be valuable to also quantify their intercellular oxygen levels to better control the post-harvest storage conditions.

One of the main limitations of the GASMAS technique is that the GASMAS signal is not only influenced by the gas concentration, but also by the path length travelled through the medium (Mei et al., 2014). Light propagation through fruit tissues is the result of a complex interplay of light scattering and light absorption. The amount of scattering depends on the structure and density of cellular components, whereas the absorption is mainly caused by the presence of different chemical compounds. Light propagation simulations can provide insight into the light-tissue interaction in scattering media. The Monte Carlo (MC) method is suitable to simulate tissue layers with arbitrary optical parameters. The potential of MC simulations to predict light transport through fruit tissues has already been demonstrated for apple (Vaudelle and L'Huillier, 2015) and peach (Ding et al., 2015). In the context of GASMAS sensing, MC simulations could help to understand the light-tissue interaction and model the relation between the oxygen concentration in a diffuse medium and the GASMAS signal.

Given the importance of non-destructive intercellular O_2 measurements for CA storage and the lack of reports on GASMAS application in low porosity fruit like pear, the aim of this study was to validate and evaluate a GASMAS O_2 sensor for monitoring of the oxygen concentration in pome fruits. It builds on the sentinel discovery work on non-destructive measurement of oxygen diffusion in apples reported by Persson et al. (2006) and extends it to respiration studies in intact pome fruit with different porosities with and without edible coating.

In the first part, the performance of the GASMAS sensor is validated using an Intralipid® liquid phantom model with a range of O_2 levels and scattering values covering typical values for pome fruit skin and flesh. MC simulations are used to obtain insight in the light propagation through the diffuse media and optimize the design of the model systems. In the second part, the applicability of the GASMAS sensor is evaluated on pome fruit with high and low porosity to study the relation between fruit porosity and O_2 depletion due to respiration. As edible coatings are often used in post-harvest storage, their effect on diffusion resistance is also studied

2. MATERIALS AND METHODS

2.1 GASMAS oxygen sensor

A non-destructive O_2 sensor (GasSpect™, GASPOROX AB, Sweden) operating according to the TDLAS principle (Linnerud et al., 1998) was used in the current study. The compact portable sensor is configured in transmitter-receiver format. The transmitter box consists of a tunable diode laser source (0.044 W), laser control module and a collimating lens package. A large area Si photodetector (10 mm^2) and receiver electronics are the main components of the receiver box. The system measures the average O_2 partial pressure along the optical line-of-sight where the O_2 in the air between the laser source and the sample was removed by nitrogen flushing. While performing measurements with the model systems, the diffuse transmitted light was detected by placing the transmitter and receiver boxes opposite to each other. In the case of fruit, a diffusively

reflected signal was collected by positioning the source and detector module in a 45° angle configuration (Figure 1). Laser light scanned across the absorption line of oxygen (760 nm), while the receiver unit continuously monitored the changes in light intensity. The system output is corresponds to optical path length (m) times the O_2 partial pressure (kPa).

2.2 Simulation of GASMAS signal for multilayer model systems

A multilayer tissue mimicking model system was designed for validating the accuracy of the GASMAS sensor in measuring the concentration of O_2 gas in a turbid medium. Monte Carlo (MC) simulations were performed to quantify the fraction of photons transmitted through the model system for different combinations of thickness and bulk optical properties (BOP) of the model layers. The MC simulations were run in Matlab (2018) for a total of 4×10^6 photons with a Gaussian beam profile for an irradiation wavelength at 760 nm. The photons irradiated on the first phantom layer are diffusively transmitted to the middle gas layer. Here a fraction of the photons are absorbed, while the remaining ones are diffusively transmitted through the third phantom layer. The influence of scattering on the light propagation was studied by changing the phantom layer's bulk scattering coefficient (μ_s) from 20 cm^{-1} to 200 cm^{-1}. The bulk absorption coefficient (μ_a) of the gas layer (0.0002 cm^{-1}) was set to the value for oxygen at 760 nm (Tian et al., 2009). The bulk optical properties considered in the simulation are summarized in Table 1. For simulation models of varying scattering and O_2 layer thicknesses, the light propagation was quantified in terms of reflection, absorption and transmission. Further, the influence of phantom layer scattering on the laser irradiance was studied for three chosen scattering (μ_s) levels: 20 cm^{-1},100 cm^{-1} and 200 cm^{-1}.

Table 1. Optical properties used in the MC simulations for the propagation of photons with a wavelength of 760 nm through the model system. μ_s = bulk scattering coefficient; μ_a = bulk absorption coefficient; g = anisotropy factor; n = refractive index.

Layers	μ_s (cm^{-1})	μ_a (cm^{-1})	g	n	Thickness (m)
Liquid phantom	20; 100; 200	0.0	0.9	1.36	0.004
Oxygen	0.0	0.0002	1	1	0.02, 0.05, 0.10

148

149 **2.3 Evaluation of GASMAS oxygen sensor**

150 **2.3.1 Model systems**

151 Based on the MC simulations, a physical model system consisting of two liquid Intralipid®
152 phantom layers and a central O_2 layer was designed to validate the performance of the GASMAS
153 sensor in porous media. The side phantom layers consisted of transparent 0.05 x 0.05 x 0.004 m
154 glass cuvettes and in between these cuvettes a gas layer was built by using an open ended plastic
155 tube which was tightly glued in between two glass cuvettes. Model systems with three different
156 O_2 layer thicknesses including 0.02 m, 0.05 m, and 0.10 m were used to investigate the effect of
157 the path length in gas on the GASMAS signal. A gas mixing panel was used to prepare gas
158 sampling bags with different O_2 partial pressures: 0.01 kPa, 0.2 kPa, 0.5 kPa and 1 kPa. Two
159 valves were used to control the in- and outflow of O_2 in the model system. Different Intralipid®
160 (Fresenius Kabi, Germany) volume concentrations (Q_p) were used to prepare solutions of three
161 different scattering levels (μ_s): 20 cm^{-1}, 100 cm^{-1} and 200 cm^{-1} (Aernouts et al., 2014):

162 $$\mu_s = \frac{{\mu_s}^{indep}}{0.227} \times Q_P \times \frac{1-{Q_P}^{P(\lambda)+1}}{[1+Q_P\,(P(\lambda)-1)]^{P(\lambda)-1}} \quad (2)$$

163 $${\mu_s}^{indep} = 1.868 \times 10^{10} \times \lambda^{-2.59} \quad (3)$$

164 $$P(\lambda) = 1.31 + 0.0005481\lambda \quad (4)$$

165 Here, λ is wavelength in nm, ${\mu_s}^{indep}$ is the independent scattering and $P(\lambda)$ is the packing factor
166 at wavelength λ. The scattering properties of the different Intralipid® solutions were also verified

using double integrating spheres (DIS) measurements, as described by Aernouts et al. (2014). For each Intralipid® solution, four different O_2 partial pressures were tested. For each Intralipid® scattering-oxygen combination, the measurement was repeated three times and after each measurement the gas chamber was flushed with nitrogen gas. As the length of each gas layers are known, the oxygen concentration extracted from the obtained GASMAS signal (gas concentration times the path length. Thereafter measured O_2 partial pressure plotted against the reference O_2 partial pressure for different phantom scatterings.

2.3.2 Fruit materials

Three economically relevant pome fruit with different porosity which are mainly stored under CA, being 'Golden delicious' and 'Nicoter' apples (*Malus* x *domestica* Borkh.), and 'Conference' pear (*Pyrus communis* L.) were selected and collected from a local supermarket in Belgium. Three samples of each cultivar were used in the GASMAS measurements.

2.4.2 BioFresh™ coating and oxygen diffusion studies

In this study, 1.2 % of BioFresh™ powder (Bel' Export, Belgium) was used to prepare the coating solution in order to study the difference in diffusion resistance of a coated 'Golden delicious' apple and 'Conference' pear compared to their uncoated counterparts. The fruit were dipped in the prepared solution for a few minutes and then air dried. Afterwards, the BioFresh™ coated, uncoated and peeled fruit were kept in three different gaseous nitrogen-filled jars for 2 h. Immediately after taking the samples from the jars, the evolution of the O_2 partial pressure in the fruit was measured with the GASMAS O_2 sensor until the GASMAS signal reached an equilibrium value. The data was collected at a frequency of 3.28 Hz. As the GASMAS signal is influenced by both the path length travelled through the tissue and the O_2 partial pressure in the intercellular space, a change in O_2 partial pressure cannot be distinguished from a change in path length. Therefore, the measured signals were converted in a relative O_2 partial pressure values,

calculated as the ratio of the GASMAS signal over the equivalent path length (L_{eq}). The latter was estimated as the GASMAS signal measured for the same fruit when it was in equilibrium with the atmospheric oxygen concentration of 20.9 %. The time evolution of these relative O_2 partial pressure was then fitted with an exponential function to estimate the time constant, defined as the time required to reach 1/e of the equilibrium value.

2.4.3 Oxygen depletion due to respiration

When the oxygen consumption for respiration is larger than the oxygen diffusion into the fruit, the oxygen gas in the intracellular spaces will be depleted. To quantify the effect of fruit porosity on this oxygen depletion due to respiration, pome fruit with two very different porosities, namely a 'Golden Delicious' apple and a 'Conference' pear were submerged in water with an average temperature of 19°C for 15 min. It was expected that the very low dissolved O_2 content in the water would minimize the entry of oxygen gas into the fruit (Ibanez et al., 2008), resulting in a decrease in the intracellular O_2 partial pressure. Immediately after taking the fruit out of the water, measurements were performed with the GASMAS O_2 sensor for 2 min. Afterwards, fruit were placed back in the water for another 15 min. This procedure was repeated for 3 h. The relative O_2 consumption was calculated from the observed GASMAS signals as explained in section 2.4.2.

3. RESULTS

3.1 Effect of model system design on light propagation studied by MC simulations

In Figure 2, the light propagation through the multilayer turbid model system simulated with an MC simulation is illustrated. The detected power is estimated as the product of the laser output power (0.044 W) and the relative transmission or the relative reflection. As expected, when the Intralipid® phantom's bulk scattering coefficient (μ_s) increased from 20 cm^{-1} to 200 cm^{-1}, the diffuse transmittance (T_d) through the model system was greatly reduced and this reduction was even larger in thicker (0.02 m) phantom layers. With a decrease in phantom layer thickness from 0.02

m to 0.002 m, approximately a 4-fold increase in detected power was observed. The majority of the photons was absorbed in the middle gas layer. As illustrated in Figure 2.B, the power absorbed (absorption times the laser power) at 760 nm increased with layer thickness. Moreover, the absorbed power slightly increased when the Intralipid® phantom layer scattering (μ_s) increased from 20 cm^{-1} to 200 cm^{-1}. In Figure 3, the variation in the intensity distribution is illustrated for multi-layered model systems with different phantom layer scattering values. As the bulk scattering coefficient (μ_s) increases from 20 cm^{-1} to 200 cm^{-1}, a large portion of the photons diffuses in the first phantom layer itself which thus reduces the intensity distribution in the subsequent layers. It is also apparent from the simulations that the intensity distribution reduces with layer thickness and the maximum intensity is found near the point of illumination.

3.2 GASMAS oxygen sensor validation in scattering media

In Figure 4, the results of the validation of the GASMAS O_2 sensor are illustrated for the Intralipid® phantom models measured in transmittance mode. As illustrated in Figure 4.A, a significant increase in GASMAS signal intensity was noticed when the O_2 partial pressure increased from 1 % to 100 %. Moreover, this effect seems to be linear as the signal intensity approximately doubled when the O_2 partial pressure increased from 50 % to 100 %. It is also important to note that the system could measure O_2 partial pressure as low as 1 % even though the detected signal was more noisy. From the GASMAS signal, the O_2 partial pressure were estimated by considering the physical length of the O_2 layers (0.02 m, 0.05 m and 0.10 m) to make a calibration graph for three different scattering conditions, as shown in Figure 4.B to 4.D. The calculated O_2 partial pressure are linearly correlated ($R^2 \geq 0.9$) with the reference O_2 partial pressures. However, by increasing the Intralipid® scattering value (μ_s) from 20 cm^{-1} to 200 cm^{-1}, the calculated O_2 partial pressure increased by around 10 %. This is in agreement with the effect of scattering level on the intensity of the absorption signal calculated from the MC simulations (Figure 2.B). Moreover, this difference O_2 partial pressure is more clearly visible for the 0.02 m model system than for the 0.05

m and 0.10 m systems. This indicates that the equivalent path length travelled through the O_2 layer depends on the scattering level of the surrounding tissue. In apple, for example, this is related to the size and density of the pores (Wang et al., 2020).

3.3 Relation between fruit porosity and TDLAS signal

As the attenuation of a light beam travelling through a thick layer of highly scattering tissue is very high, the power of the light transmitted through the fruit was too low to obtain reliable signals. Therefore, the pome fruit were measured in diffuse reflectance mode, as illustrated in Figure 1. In Figure 5, the GASMAS signal obtained from 'Golden delicious' apples, 'Nicoter' apples and 'Conference' pears is shown. As the GASMAS signal is influenced both by the path length travelled through the tissue and the O_2 partial pressure in the intercellular space, a change in O_2 partial pressure cannot be distinguished from a change in path length. Therefore, the measured signal is expressed in terms of equivalent path length (L_{eq}), the path length measured for a fruit in equilibrium with the atmospheric O_2 partial pressure. The L_{eq} calculated for 'Golden delicious' apples was nearly 5 times longer than the value calculated for the 'Conference' pears and more than 2 times longer than for the 'Nicoter' apples. Similar relations were observed for the porosity of similar pome fruit (Ting et al., 2013; Ho et al., 2010), where 'Golden delicious' (29 ± 0.8 %) was 5 times more porous than 'Conference' pear (6 ± 1%) and nearly 2.5 times more than 'Nicoter' apple (12 ± 0.5%) (Verboven et al., 2008). Moreover, the L_{eq} estimated for the 'Golden delicious' apple was approximately 4 times longer than the maximum source detector separation (0.02 m), and for 'Nicoter' it was around 2 times longer. However, in the case of the 'Conference' pear the difference was negligibly small.

3.4 Reduced oxygen diffusion due to BioFresh™ coating

The diffusion dynamics observed after 2 h of nitrogen treatment for a peeled, unpeeled and BioFresh™ coated 'Golden delicious' apple and 'Conference' pear are illustrated in **Error!**

Reference source not found.. The estimated diffusion time constant for the BioFresh™ coated 'Golden delicious' apple is much longer (103 min) than for the uncoated (51.5 min) and peeled (27.2 min) samples. A similar trend can be observed for the 'Conference' pears although the estimated time constants were comparatively smaller in all three tested conditions. The peeled and unpeeled 'Golden delicious' apples started off with the same O_2 partial pressure levels after 2 h of nitrogen treatment, whereas the BioFresh™ coated sample did not reach the same starting point as the peeled and unpeeled samples. This suggests that the BioFresh™ coating also hampered the nitrogen purging from the intercellular spaces. However, this hypothesis was not confirmed in case of the 'Conference' pear, where the starting point fluctuated in all three tested conditions.

3.5 Respiration measurements for two different porosity fruit

In Figure 7, the evolution of the O_2 partial pressure after submerging samples in water is illustrated for a 'Golden delicious' apple and a 'Conference' pear. The indicated concentration values are an averages of 2 min measurement. It should be noted that the 'Conference' pear consumed the intercellular O_2 faster than the 'Golden delicious' apple. The Conference pear reached an equilibrium state after 80 min, whereas the 'Golden delicious' apple took more than 180 min to reach the equilibrium state. Also be noted that the rate of O_2 consumption in both fruit decreased gradually with time. This can be attributed to the dependence of the respiration rate on the O_2 partial pressure (Kays, 1991).

4. DISCUSSION

Tissue simulating aqueous phantoms are commonly used for validating spectroscopic applications in diffuse media (Ohmae et al., 2018). The Intralipid® liquid phantom models used in this study were a coarse approximation of a porous turbid medium involving both scattering layers and a gas phase to validate the GASMAS sensor performance in measuring the O_2 partial

pressure in porous tissues. As the thickness and BOP of tissue layers have a large influence on the interaction of laser light with tissue (Raulin and Karsai, 2011), a Monte Carlo light propagation model (Song et al., 2013; Watté et al., 2015) was used to optimize the layer thickness of the phantom models. The selected phantom layer thickness (0.004 m) for our model was appropriate to measure O_2 in diffuse transmission geometry even with high scattering (μ_s: 200 cm^{-1}). When the thickness of the scattering layer increased to 0.02 m, barely any transmitted light could be detected, especially for the high scattering levels (μ_s: 100 cm^{-1} and μ_s: 200 cm^{-1}), which was in-line with the simulation results (Figure 3). To overcome this limitation, Persson et al. (2007) recommended to measure thicker samples with high scattering properties in diffuse reflectance mode. The three layers considered in the proposed model system were either purely scattering or absorbing. The two outer layers filled with Intralipid® mimic the highly scattering fruit skin, while the middle layer, dominated by absorption, represents a very rudimental model of the porous fruit cortex. However, in real fruit both of these optical events occur in a single tissue layer where the incident light on the tissue surface propagates diffusely due to the strong scattering from the cellular components, while photons are absorbed by the oxygen gas in the intercellular pores (Vaudelle and L'Huillier, 2015; Svanberg, 2013). The model system used in this study does not mimic the air-filled porous structures of fruit cortex correctly. Therefore, it is recommended to define layers with mixed scattering and absorption features in future work in order to create a solid porous model system that is more representative for the internal structure of pome fruit. The design of such a model system could also be optimized through the use of more advanced MC simulations.

The bulk scattering coefficient (μ_s) values of the prepared diffusion solutions were close to the μ_s values reported for apple skin and flesh, respectively 200 cm^{-1} and 100 cm^{-1} (Van Beers et al., 2017). The scattering solutions were prepared according to Eqns. (2)-(4) and were verified with the DIS method which showed only a slight variation (± 5 cm^{-1}) from the theoretical value. We

speculate that this small deviation might be due to inaccurate solution preparation and mixing. As the middle gas layer is purely absorbing and its thickness is directly related to the absorption signal intensity (Beer-Lambert law), three layer thicknesses including 0.02 m, 0.05 m and 0.10 m were selected for sensor validation. When light interacts with the first phantom layer, part of the light undergoes specular and diffuse reflection, while the transmitted light travelled straight through the gas layer where a fraction of it was absorbed depending on the concentration of O_2 molecules. Then, the remaining light goes to the third layer where it is scattered, resulting in a part of the light being reflected back into the gas layer and a part being transmitted. This results in variation in the average path length that the photons travel through the gas layer. Therefore, the intensity measured by the detector is influenced both by the effective optical path length and the O_2 partial pressure. However, the measured O_2 partial pressure (Figure 5.B-5.D) was calculated based on the physical length of the gas layer instead of the effective optical path length which is generally higher for high scattering media (Svanberg, 2013). This could explain the high offset with a μ_s of 200 cm^{-1} compared to 20 cm^{-1}. A less accurate O_2 partial pressure measurement was noticed at low concentration (1%), suggesting that the sensor is less precise for low O_2 partial pressures. A similar conclusion was reported by Cocola et al. (2016) for TDLAS O_2 sensor validation on flow packages. Inefficient gas mixing may also have contributed to the increased offset in the low concentration measurements. Persson et al. (2007b) demonstrated a phantom model made up of two scattering polymeric Delrin-materials (μ_s ~140 cm^{-1}) which were separated by various air distances to validate the GASMAS O_2 sensor for application in the human sinus. In comparison with those models, the current Intralipid® liquid phantom model was more efficient to investigate the feasibility of the sensor in different scattering environments, including μ_s of 20 cm^{-1},100 cm^{-1} and 200 cm^{-1}. Also, the present model is not only focusing on the influence of path length on the TDLAS signal intensity, but also the effect of different O_2 partial pressure on the signal strength.

Although both pear and apple are climacteric fruit, pears are more prone to hypoxia-related physiological disorders in CA storage (Ho et al., 2008). The evolution in the O_2 gas concentrations measured in both pear and apple tissues using the non-destructive GASMAS O_2 sensor provide interesting insights with respect to this. Even though the current system was limited to the detection of diffuse reflected signals and the estimated O_2 partial pressure were only representative for a small part of the intact fruit, it provides valuable information on the variation in GASMAS signal between and within apples and pears. When laser light interacts with the fruit, the light undergoes high scattering from its skin and then the diffuse light is transmitted through the gas pores of the tissue (Wang et al., 2020). Light may take a long path through the scattering tissue and so the detected absorption signal of unknown path length cannot provide an absolute O_2 partial pressure according to the Beer-Lambert law. Due to this limitation, the TDLAS O_2 measurement expressed in terms of equivalent path length (L_{eq}) had to be related to the 20.9 % of O_2 in the ambient air (Figure 6). The higher L_{eq} values obtained for the apple samples can both be interpreted as an indication of a higher O_2 partial pressure in the intercellular cavities or a larger path length through the large porous cavities. As the L_{eq} obtained for the apple samples was much larger than that of the set maximum source and detector separation (~0.02 m), it is hypothesized that the high L_{eq} is rather the result of a larger path through the porous cavities in highly porous apple tissue than of a higher internal O_2 partial pressure. Moreover, the L_{eq} values observed for the 'Golden delicious' apples were larger than those for the 'Nicoter' apples, which is in line with the differences in porosity and void structures in terms of pore distribution and connectivity reported by Verboven et al. (2008). Contrary to these findings, Persson et al. (2006) reported similar L_{eq} values for slabs of different apple varieties including 'Jonagold', 'Granny Smith', 'Red Delicious', 'Golden Delicious' and 'Royal Gala'. The intercellular spaces in pear tissue are much smaller than in apple tissue and highly interconnected (Ho et al., 2008). This might be the explanation for the lower GASMAS signals obtained for the pear samples and could explain the low L_{eq} values obtained for the pear samples.

As there is an inverse relation between the respiration rate and post-harvest life, application of the GASMAS technique for non-destructive fruit respiration measurement could provide a remarkable contribution to the growing research on dynamic control storage (DCA). Generally, atmospheric O_2 diffuses into the intercellular space through the skin and then subsequently reaches the cells where it is utilized for cellular respiration (Ho et al., 2008). Gas diffusion is mainly driven by the concentration gradient according to Fick's law. When fruit are dipped in water, where the dissolved O_2 partial pressure is very low, approximately 1% compared to the 20.9 % O_2 in the air (Ibanez et al., 2008), the normal gas exchange of fruit is interrupted, while respiration continues. Gradually with time, the fruit consumes the O_2 available in the cells and intercellular spaces to keep the cells alive. Therefore, the decrease in O_2 partial pressure in water submerged fruit is most likely driven by their respiration level. The relative rate of O_2 consumption in pear was faster than that in the apple samples, when they were water submerged and a measurement was performed every 15 min for 3 h (Figure 7). The lower volume of air in the 'Conference' pear cortex tissue compared to the 'Golden delicious' apple cortex might be the reason for the faster O_2 depletion in pear (Herremans et al., 2015). However, it could also be an indication of faster respiration in pear compared to apple, which was suggested by Ho et al., (2018) from a mathematical model based study. However, it should be noted that in this study the samples were taken out of the water for each measurement, which may have elongated the time to reach the equilibrium state. Therefore, it is recommended to avoid this exposure to ambient air during the measurements in future studies.

From a gas diffusion study on fruit, Ho et al. (2008) concluded that gas diffusion depends on microstructural properties including porosity, connectivity and cell distribution. To verify the porosity dependent O_2 diffusion, a 'Golden delicious' apple and 'Conference' pear were submerged in nitrogen for 2 h and then the O_2 re-inversion was observed. Additionally, peeled and BioFresh^{TM} coated samples were considered to verify the influence of skin and an additional

skin coating on diffusion. As fruit skin acts as a barrier for gas diffusion, the diffusion time constants of both peeled 'Golden delicious' apple and 'Conference' pear were smaller than those for the unpeeled and BioFresh^{TM} coated samples. Moreover, in all three conditions, the diffusion time constants for pear were found to be smaller than those for the apple samples. This confirms that the gas diffusion in fruit depends on its tissue properties (Ho et al., 2008). Although 'Golden delicious' apples are more porous than 'Granny Smith' apples (Ting et al., 2013; Ho et al., 2010), the diffusion time constant observed in this study for 'Golden delicious' apples was more than 2 times larger than the values reported by Persson et al. (2006) for 'Granny Smith' apples. This difference might be partially attributed to the longer nitrogen treatment of the 'Granny Smith' apples in the study of Persson et al. (2006) (24 h) compared to the 2 h nitrogen treatment in the present study. The obtained results also confirm that the addition of an edible coating increased the diffusion resistance by blocking the pores partially or completely. The increased gas diffusion resistance with coating is expected to reduce the respiration, which may help to prolong the shelf-life of fruit if it does not lead to hypoxia in the inner fruit tissue. As fruit has O_2 partial pressure gradient from its center towards the surface, understanding of this spatial O_2 gradient will give more insight into the postharvest biology of fruit. Especially help to understand hypoxia-related internal disorders (eg. Internal browning) which are common in CA stored fruit. Therefore, the feasibility GASMAS technique for intact fruit oxygen spatial distribution mapping will be evaluated in future research.

5. CONCLUSIONS

In this study, the application of a GASMAS sensor was validated and evaluated for non-destructive intercellular O_2 measurement in pome fruit. A fruit mimicking Intralipid® liquid phantom based model system provided insight into the relation between the O_2 partial pressure and the signals acquired with the GASMAS sensor in scattering media. Measurements on economically relevant pome fruit samples including 'Golden delicious' apples, 'Nicoter' apples and 'Conference'

pears provided insight in the variation in the GASMAS signals acquired on different fruit, which could be attributed to the differences in the porosity of these fruit. When the fruit were submerged in water, the O_2 partial pressure was found to decrease much faster in the pear samples than in the apple samples. This could partly explain why pears are more sensitive to hypoxia related storage disorders. It was also confirmed that the fruit skin acts as a barrier layer and removal of the skin reduced the gas diffusion resistance. A slower diffusion was observed with a BioFresh^{TM} coating on both pears and apples, confirming the potential of such coatings for respiration reduction and retaining the fruit quality throughout storage life if the fruit do not suffer from hypoxia. The obtained results confirm the potential of GASMAS sensors for non-intrusive gas measurement in porous tissues, especially for the intracellular O_2 measurement in porous fruit like apple and pear. This opens up possibilities for the use of GASMAS O_2 sensing to reduce hypoxia related internal disorders in CA storage, thereby improving quality and shelf life of stored pome fruit.

ACKNOWLEDGEMENT

The authors would like to thank Märta Lewander Xu and Patrik Lundin from GASPOROX AG, Sweden, for taking part in the discussion and lending their setup for our experiment. This work was financially supported by KU Leuven internal funding (C1 project -3E160393).

REFERENCES

Aernouts, B., Van Beers, R., Watté, R., Lammertyn, J., Saeys, W., 2014. Dependent scattering in Intralipid® phantoms in the 600-1850 nm range. Opt. Express 22, 6086. https://doi.org/10.1364/oe.22.006086.

Armstrong W, Cringle S, Brown M, Greenway H ,1993. A micro-electrode study of oxygen distribution in the roots of intact maize seedlings, In: Jackson MB, Black CR (eds) Interacting stresses on plants in a changing climate, vol 16, NATO ASI Series 1. Springer, Berlin, pp 287–304.

Bessemans, N., Verboven, P., Verlinden, B.E., Nicolaï, B.M., 2016. A novel type of dynamic controlled atmosphere

storage based on the respiratory quotient (RQ-DCA). Postharvest Biol. Technol. 115, 91–102. https://doi.org/10.1016/j.postharvbio.2015.12.019

Boonruang, B.K., Chonhenchob, V., Singh, S.P., 2012. PAPER PRESENTED AT IAPRI SYMPOSIUM 2011 , BERLIN Comparison of Various Packaging Films for Mango Export 107–118. https://doi.org/10.1002/pts

Busatto, N., Tadiello, A., Trainotti, L., Costa, F., 2017. Climacteric ripening of apple fruit is regulated by transcriptional circuits stimulated by cross-talks between ethylene and auxin. Plant Signal. Behav. 12, 1–4. https://doi.org/10.1080/15592324.2016.1268312

Ding, C., Shi, S., Chen, J., Wei, W., Tan, Z., 2015. Analysis of Light Transport Features in Stone Fruits Using Monte Carlo Simulation. PLoS One 10, e0140582. https://doi.org/10.1371/journal.pone.0140582 PM - 26469695

Ding, Y., Lin, H., Yan, C., n.d. Methane detection studies based on gas in scattering media absorption spectroscopy. Asia Commun. Photonics Conf. 2014. https://doi.org/10.1364/ACPC.2014.ATh3A.190

Herremans, E., Verboven, P., Verlinden, B.E., Cantre, D., Abera, M., Wevers, M., Nicolaï, B.M., 2015. Automatic analysis of the 3-D microstructure of fruit parenchyma tissue using X-ray micro-CT explains differences in aeration. BMC Plant Biol. 15, 1–14. https://doi.org/10.1186/s12870-015-0650-y

Ho, Q.T., Verboven, P., Verlinden, B.E., Lammertyn, J., Vandewalle, S., Nicolaï, B.M., 2008. A continuum model for metabolic gas exchange in pear fruit. PLoS Comput. Biol. 4, e1000023. https://doi.org/10.1371/journal.pcbi.1000023 PM - 18369422

Ho, Q.T., Verboven, P., Verlinden, B.E., Schenk, A., Nicolaï, B.M., 2013. Controlled atmosphere storage may lead to local ATP deficiency in apple. Postharvest Biol. Technol. 78, 103–112. https://doi.org/10.1016/j.postharvbio.2012.12.014

Ibanez, J.G., Hernandez-Esparza, M., Doria-Serrano, C., Fregoso-Infante, A., Singh, M.M., 2008. The Point of Zero Charge of Oxides In: Environmental Chemistry 70–78. https://doi.org/10.1007/978-0-387-49493-7

Kays, S.J., 1991. Postharvest Physiology of Perishable Plant Products. Postharvest Physiol. Perish. Plant Prod. 1991. https://doi.org/10.1007/978-1-4684-8255-3

Linnerud, I., Kaspersen, P., Jæger, T., 1998. Gas monitoring in the process industry using diode laser spectroscopy. Appl. Phys. B Lasers Opt. 67, 297–305. https://doi.org/10.1007/s003400050509

Mei, L., Somesfalean, G., Svanberg, S., 2014. Pathlength determination for gas in scattering media absorption

spectroscopy. Sensors (Switzerland) 14, 3871–3890. https://doi.org/10.3390/s140303871

Ohmae, E., Yoshizawa, N., Yoshimoto, K., Hayashi, M., Wada, H., Mimura, T., Suzuki, H., Homma, S., Suzuki, N., Ogura, H., Nasu, H., Sakahara, H., Yamashita, Y., Ueda, Y., 2018. Stable tissue-simulating phantoms with various water and lipid contents for diffuse optical spectroscopy. Biomed. Opt. Express 9, 5792.https://doi.org/10.1364/boe.9.005792

Persson, L., Andersson, M., Cassel-Engquist, M., Svanberg, K., Svanberg, S., 2007a. Gas monitoring in human sinuses using tunable diode laser spectroscopy. J. Biomed. Opt. 12, 054001. https://doi.org/10.1117/1.2777189

Persson, L., Kristensson, E., Simonsson, L., Svanberg, S., 2007b. Monte Carlo simulations related to gas-based optical diagnosis of human sinusitis. J. Biomed. Opt. 12, 54002. https://doi.org/10.1117/1.2777179 PM - 17994890

Persson, L., Gao, H., Sjöholm, M., Svanberg, S., 2006. Diode laser absorption spectroscopy for studies of gas exchange in fruits. Opt. Lasers Eng. 44, 687–698. https://doi.org/10.1016/j.optlaseng.2005.03.014

Persson, L., Kristensson, E., Simonsson, L., Svanberg, S., 2007b. Monte Carlo simulations related to gas-based optical diagnosis of human sinusitis. J. Biomed. Opt. 12, 54002. https://doi.org/10.1117/1.2777179 PM - 17994890

Raulin, C., Karsai, S., 2011. Laser and IPL technology in dermatology and aesthetic medicine. Laser IPL Technol. Dermatology Aesthetic Med. 1–419. https://doi.org/10.1007/978-3-642-03438-1

Rolletschek, H., Liebsch, G., 2017. A method for imaging oxygen distribution and respiration at a microscopic level of resolution. Methods Mol. Biol. 1670, 31–38. https://doi.org/10.1007/978-1-4939-7292-0_3

Sjöholm, M., Somesfalean, G., Alnis, J., Andersson-Engels, S., Svanberg, S., 2001. Analysis of gas dispersed in scattering media. Opt. Lett. 26, 16. https://doi.org/10.1364/OL.26.000016

Song, S., Kobayashi, Y., Fujie, M.G., 2013. Monte-carlo Simulation of Light Propagation considering Characteristic of Near-infrared LED and Evaluation on Tissue Phantom. Procedia CIRP 5, 25–30. https://doi.org/10.1016/j.procir.2013.01.005

Svensson, T., Andersson, M., Rippe, L., Svanberg, S., Andersson-Engels, S., Johansson, J., Folestad, S., 2008. VCSEL-based oxygen spectroscopy for structural analysis of pharmaceutical solids. Appl. Phys. B 90, 345–354. https://doi.org/10.1007/s00340-007-2901-6

Svensson, T., Shen, Z., 2010. Laser spectroscopy of gas confined in nanoporous materials. Appl. Phys. Lett. 96, 0–

55. https://doi.org/10.1063/1.3292210

Thompson, A.K., Bishop, D., 2016. Controlled Atmosphere Technology, Reference Module in Food Science. Elsevier. https://doi.org/10.1016/b978-0-08-100596-5.21136-0

Tian, G., Moosmüller, H., Arnott, W.P., 2009. Simultaneous Photoacoustic Spectroscopy of Aerosol and Oxygen A-Band Absorption for the Calibration of Aerosol Light Absorption Measurements. Aerosol Sci. Technol. 43, 1084–1090. https://doi.org/10.1080/02786820903170972

Tylewicz, U., Lundin, P., Cocola, L., Dymek, K., Rocculi, P., Svanberg, S., Dejmek, P., Gómez Galindo, F., 2012. Gas in Scattering Media Absorption Spectroscopy (GASMAS) Detected Persistent Vacuum in Apple Tissue After Vacuum Impregnation. Food Biophys. 7, 28–34. https://doi.org/10.1007/s11483-011-9239-7

van Dongen, J.T., Licausi, F., 2014. Low-Oxygen Stress in Plants. Springer Vienna, Vienna. https://doi.org/10.1007/978-3-7091-1254-0

Vaudelle, F., L'Huillier, J.-P., 2015. Influence of the size and skin thickness of apple varieties on the retrieval of internal optical properties using Vis/NIR spectroscopy: A Monte Carlo-based study. Comput. Electron. Agric. 116, 137–149. https://doi.org/10.1016/j.compag.2015.06.009

Verboven, P., Kerckhofs, G., Mebatsion, H.K., Quang, T.H., Temst, K., Wevers, M., Cloetens, P., Nicolaï, B.M., 2008. Three-dimensional gas exchange pathways in pome fruit characterized by synchrotron X-ray computed tomography. Plant Physiol. 147, 518–527. https://doi.org/10.1104/pp.108.118935

Wang, Z., Van Beers, R., Aernouts, B., Watté, R., Verboven, P., Nicolaï, B., Saeys, W., 2020. Microstructure affects light scattering in apples. Postharvest Biol. Technol. 159, 110996. https://doi.org/10.1016/j.postharvbio.2019.110996

Zhang, H., Huang, J., Li, T., Wu, X., Svanberg, S., Svanberg, K., 2014. Studies of tropical fruit ripening using three different spectroscopic techniques. J. Biomed. Opt. 19, 67001. https://doi.org/10.1117/1.JBO.19.6.067001 PM - 24887745

Zhang, H., Svanberg, S., 2016. Laser spectroscopic studies of gas diffusion in alumina ceramics. Opt. Express 24, 1986–1998. https://doi.org/10.1364/OE.24.001986 PM - 26906775

Figure captions

519 Figure 1. Schematic drawing of source (S) and detector (D) position in front view for the
520 measurement setup for the model systems (A) and fruit (B).

521 Figure 2. Effects of gas layer thickness and scattering level (μ_s) on the transmitted and absorbed
522 light intensity was studied using MC simulations for a laser source of power 44 mW at 760 nm
523 wavelength: A) Estimated diffuse transmitted (T_d) and diffuse reflected (R_d) light through the
524 Intralipid® phantom model having different phantom layer thickness and scattering values (μ_s); B)
525 Influence of gas (O_2) layer thickness on light absorption.

526 Figure 3. A: Geometry of Intralipid® liquid phantom model used in MC simulation, observed
527 irradiance (H)(W.m^2) on models of different Intralipid® scattering B: μ_s = 20 cm^{-1}, C: μ_s = 100 cm^{-1}, D: μ_s = 200 cm^{-1}.

529 Figure 4. A. Normalized GASMAS signal for different concentrations of O_2; B, C, D: calculated O_2
530 partial pressure from GASMAS measurements for different phantom scattering levels (20 cm^{-1},
531 100 cm^{-1} and 200 cm^{-1}, respectively).

532 Figure 5. Relation between equivalent path length (m) and fruit intercellular oxygen and their
533 porosity values reported by other researchers (Ting et al., 2013; Ho et al., 2010).

534 Figure 6. Observed evolution in the intercellular O_2 partial pressure after immersing samples into
535 nitrogen gas for 2 h; A: Golden delicious, B: Conference pear.

536 Figure 7. Calculated relative O_2 partial pressure from GASMAS measurement for two different
537 porosity fruit.
538

539

540

541

542

543

544

545

546

547

548

549 **Figure 1**

550

551

A

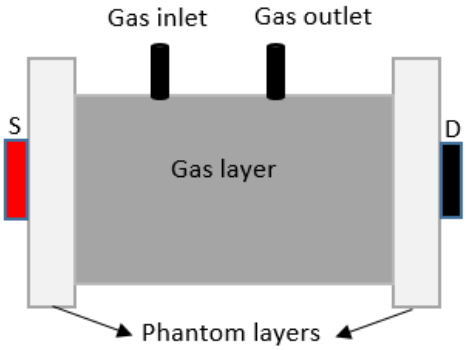

B

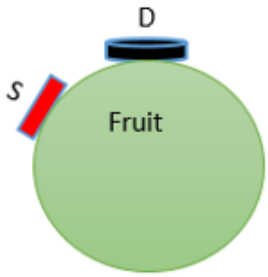

552

553

554 **Figure 2**

A

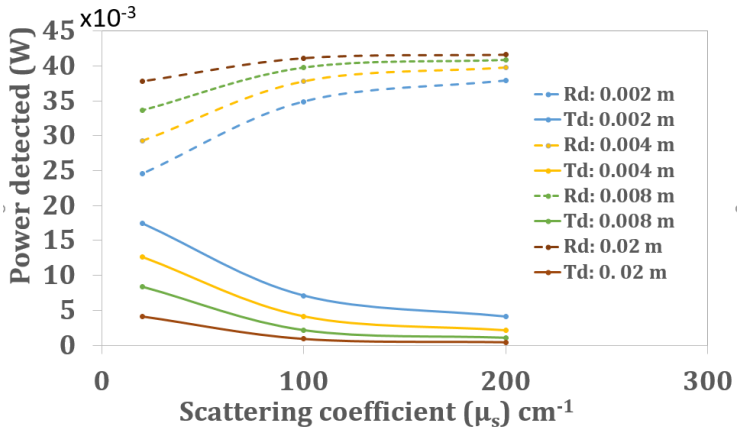

555

556

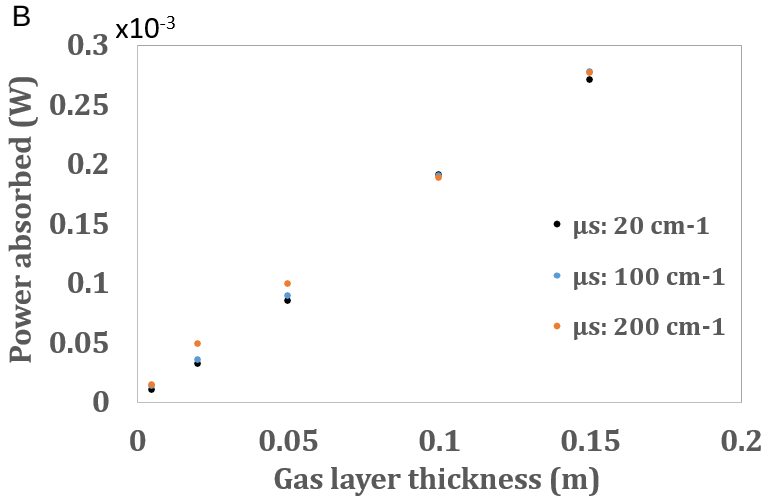

557

558 **Figure 3**

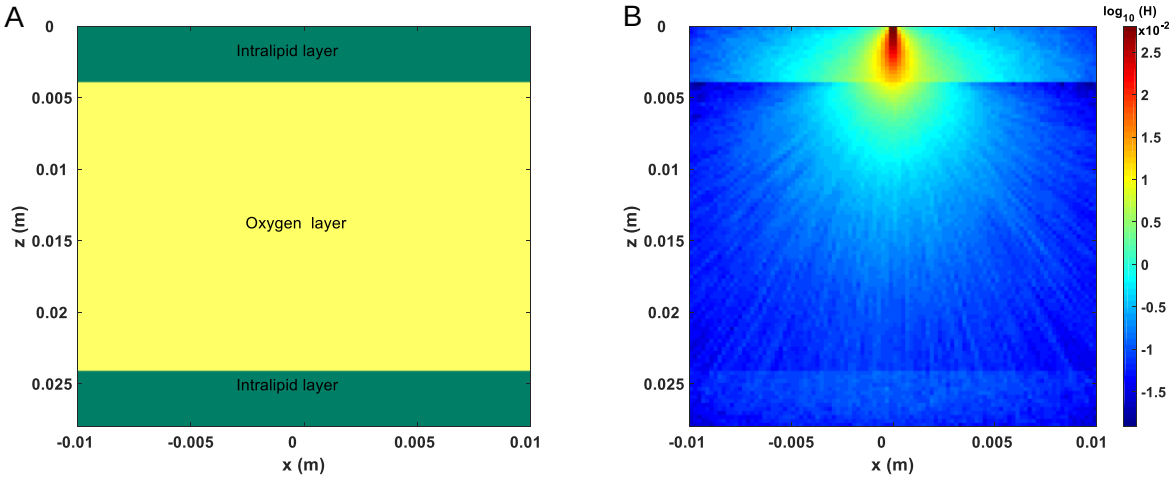

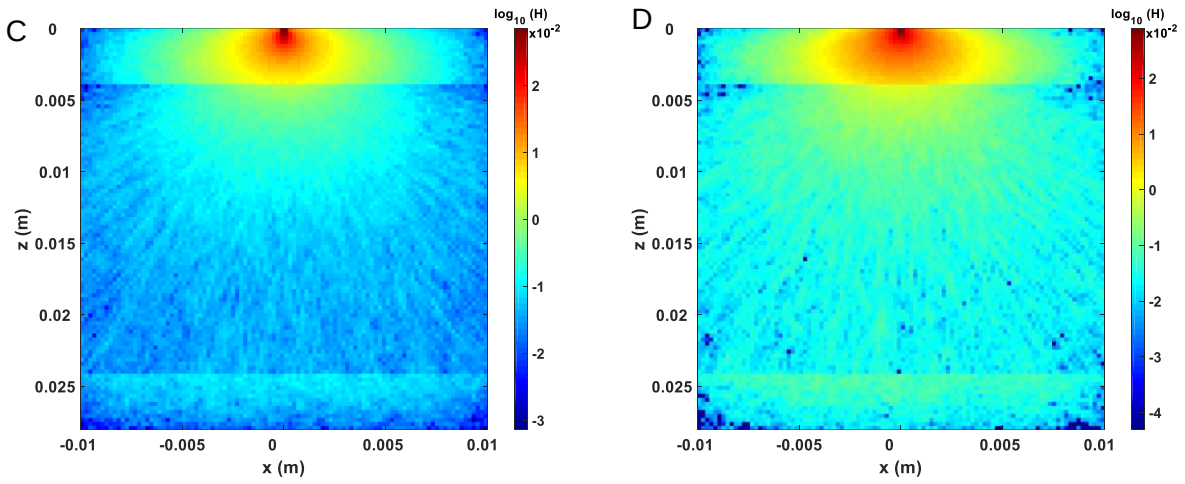

559

560 **Figure 4**

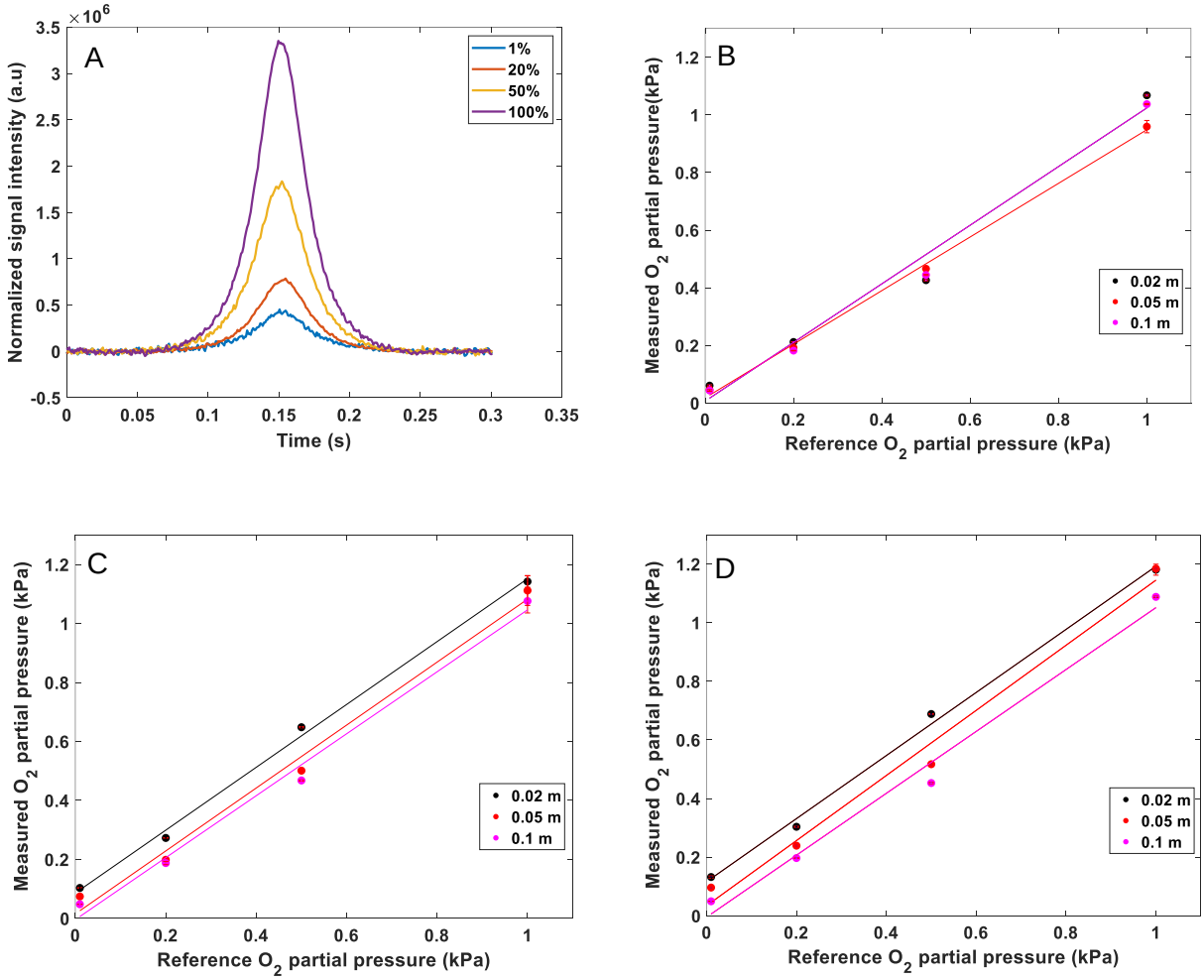

561 **Figure 5**

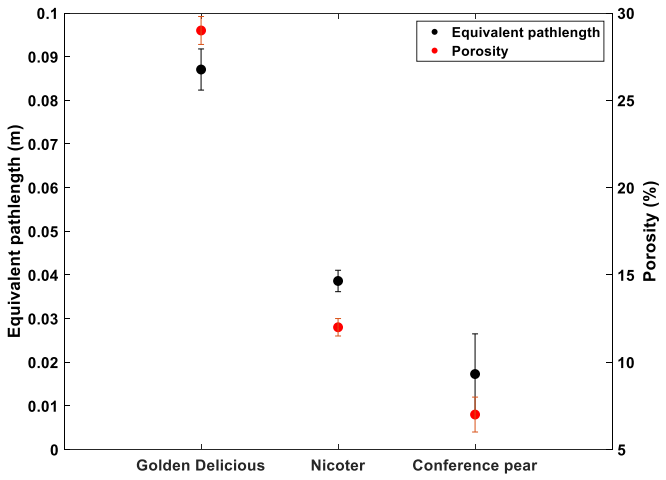

562

563 **Figure 6**

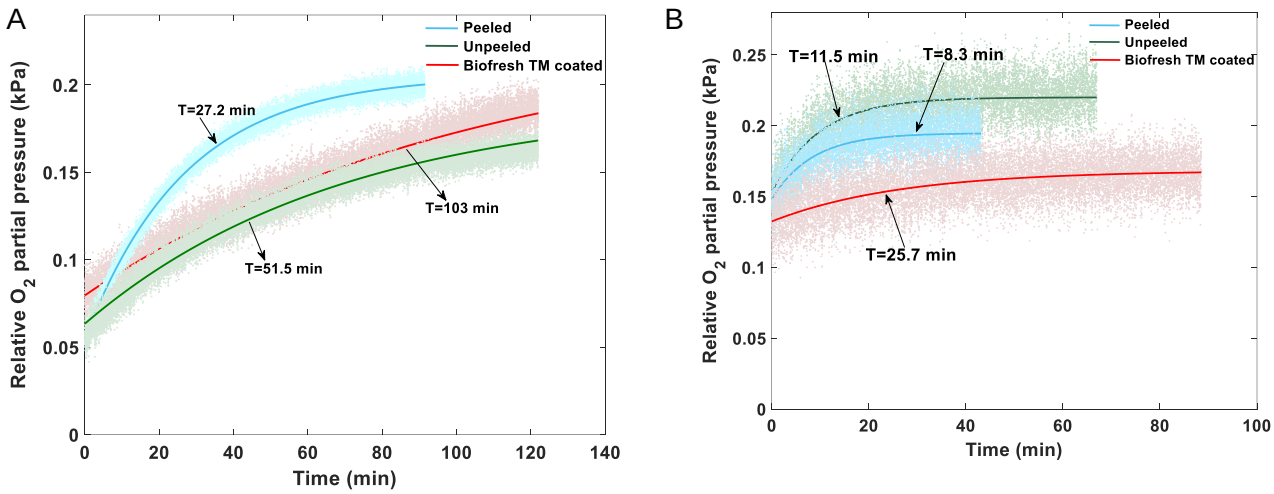

564 **Figure 7**

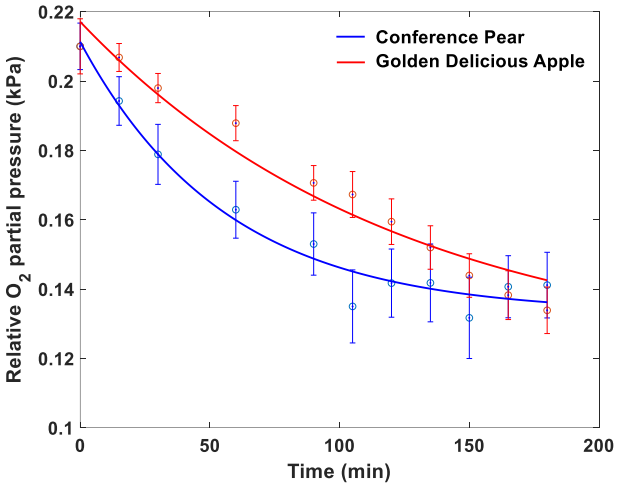
Conference Pear
Golden Delicious Apple
Relative O_2 partial pressure (kPa)
Time (min)
0.22
0.2
0.18
0.16
0.14
0.12
0.1
0
50
100
150
200

565

566